molecular pharmaceutics

pubs.acs.org/molecularpharmaceutics

Article

Effective Treatment of SSTR2-Positive Small Cell Lung Cancer Using ^{211}At-Containing Targeted α-Particle Therapy Agent Which Promotes Endogenous Antitumor Immune Response

Shanshan Qin, Yuanyou Yang, Jiajia Zhang, Yuzhen Yin, Weihao Liu, Han Zhang, Xin Fan, Mengdie Yang, and Fei Yu*

Cite This: *Mol. Pharmaceutics* 2023, 20, 5543−5553

Read Online

ACCESS | Metrics & More | Article Recommendations | Supporting Information

ABSTRACT: Small cell lung cancer (SCLC) is a neuroendocrine tumor with a high degree of malignancy. Due to limited treatment options, patients with SCLC have a poor prognosis. We have found, however, that intravenously administered octreotide (Oct) armed with astatine-211 ([^{211}At]SAB-Oct) is effective against a somatostatin receptor 2 (SSTR2)-positive SCLC tumor in SCLC tumor-bearing BALB/c nude mice. In biodistribution analysis, [^{211}At]SAB-Oct achieved the highest concentration in the SCLC tumors up to 3 h after injection as time proceeded. A single intravenous injection of [^{211}At]SAB-Oct (370 kBq) was sufficient to suppress SSTR2-positive SCLC tumor growth in treated mice by inducing DNA double-strand breaks. Additionally, a multitreatment course (370 kBq followed by twice doses of 370 kBq for a total of 1110 kBq) inhibited the growth of the tumor compared to the untreated control group without significant off-target toxicity. Surprisingly, we found that [^{211}At]SAB-Oct could up-regulate the expressions of calreticulin and major histocompatibility complex I (MHC-I) on the tumor cell membrane surface, suggesting that α-particle internal irradiation may activate an endogenous antitumor immune response through the regulation of immune cells in the tumor microenvironment, which could synergically enhance the efficacy of immunotherapy. We conclude that [^{211}At]SAB-Oct is a potential new therapeutic option for SSTR2-positive SCLC.

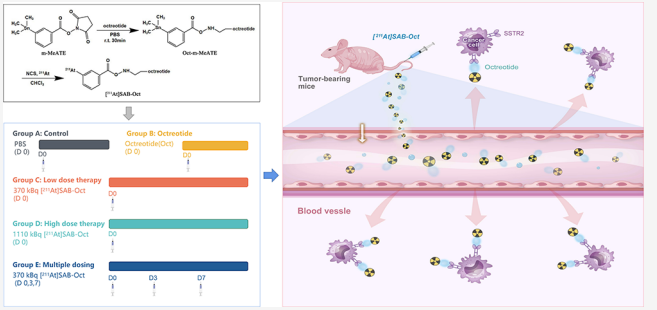

KEYWORDS: *small cell lung cancer, somatostatin receptor 2, astatine-211, octreotide, immune response*

1. INTRODUCTION

Although small cell lung cancer (SCLC) is highly sensitive to chemotherapeutic agents at the beginning of treatment, it is characterized by rapid recurrence, early widespread metastasis, and poor prognosis.[1,2] As the basic treatment of SCLC, systemic chemotherapy has reached the therapeutic plateau, and more effective treatment plans for SCLC are urgently needed.[3,4] Highly expressed somatostatin receptor (SSTR) on the surface of most SCLC cells provides an important target for nuclear medicine polypeptide-receptor-mediated radionuclide therapy (PRRT). PRRT targeting SSTR offers hope for patients with advanced SCLC who have lost the opportunity for surgery and failed to respond to other therapies.[5−7]

Octreotide is an octopeptide synthesized by the artificial modification of natural somatostatin. The peptide sequence is $_{D}$-Phe-Cys-Phe-$_{D}$-Trp-Lys-Thr-Cys-Thr-Ol (Disulfide Bridge Cys2-Cys7).[8] D-type amino acid is introduced into the structure of octreotide, which enhances the ability of resisting enzyme degradation, and the action time in vivo can be up to 2 h.[9] Most octreotide-inhibited tumor cells have one or more SSTRs on the surface, and SSTR2 is the most common.[10] The conjugate of octreotide and radionuclide can specifically bind to SSTR2 and enter tumor cells through endocytosis for targeted internal radiation therapy.[11−13] In the early stage, ^{90}Y was labeled on octreotide to play a therapeutic role.[14,15] In recent years, researchers have found that the radiation energy and half-life of ^{177}Lu, ^{225}Ac, and ^{213}Bi therapeutic nuclides are more suitable for tumor therapy than ^{90}Y, which is mainly used for the treatment of large tumors.[16−18]

^{177}Lu can release β-rays for therapeutic use, and its maximum β-ray tissue penetration is about 2 mm, which is suitable for small tumors.[19] Although the effectiveness of β-nuclides in targeted tumor therapy has been demonstrated, their use in the treatment of diffuse micrometastases has been

Received: May 16, 2023
Revised: September 15, 2023
Accepted: September 15, 2023
Published: October 3, 2023

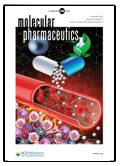

https://doi.org/10.1021/acs.molpharmaceut.3c00427
Mol. Pharmaceutics 2023, 20, 5543−5553

greatly limited. α-nuclide targeting therapy is expected to be a therapeutic method for this type of tumor.[20,21] α-nuclides are helium nuclei in nature, and their LET values are 50−230 keV/μm. The relative biological effects of α-nuclides are 3−7 times that of β-nuclides, which are shown as irreparable breaks of DNA double strands during mitosis or redistribution. The general radiation range is 28−100 μm, equivalent to the diameter of 6−8 eukaryotic cells (10−50 μm), which can significantly increase cell mortality rate per unit absorbed dose, reduce bone marrow toxicity, and limit overexposure to radiation.[22,23]

However, unlike conventional drugs and toxins, which kill only directly targeted cells, α-nuclides are unique in their ability to induce radiation-induced bystander effects or cross-fire effects. As a result, adjacent tumor cells may be destroyed even if they do not possess the specific tumor-associated receptor, enzyme, or antigen.[24] Moreover, the sensitivity of hypoxic cells to alpha ray is similar to that of normal oxygen cells, which avoids the tolerance of tumor heterogeneity to radiotherapy and overcomes the deficiency of traditional radiotherapy and chemotherapy.[25,26] Furthermore, systemically administered targeted internal irradiation therapy combines molecular-specific cell recognition with ionizing radiation's antitumor properties, possibly eliminating the primary tumor site as well as cancer that has spread throughout the body, including populations of malignant cells that are not detectable with diagnostic imaging.[27−29]

Currently, the mostly promising α-emitters are ^{211}At, ^{223}Ra, ^{213}Bi, and ^{225}Ac.[30−33] ^{225}Ac produces multiple daughter emitters, which may release from targeted carriers, leading to serious side effects caused by accidental irradiation of nontargeted tissues. The half-life of ^{213}Bi is only 46 min, which is not sufficient for drug preparation to achieve its clinical application[34]; the low stability of ^{223}Ra after chelation limits its application.[35] ^{211}At releases only one α particle, which helps reduce the off-target effects. Therefore, ^{211}At is the most promising α-emitter for clinical translation in nuclear medicine.

We successfully synthesized the octreotide SPC conjugate in the early stage,[36] which showed a good targeted therapeutic effect in the experimental study on non-small cell lung cancer (NSCLC). In the following study, we further synthesized the new octreotide ATE conjugate *N*-succinimidyl-3-[^{211}At]-astatobenzoate-Oct ([^{211}At]SAB-Oct), aiming to evaluate the growth inhibition and targeting effect of the conjugate on SCLC cell H446 and search for new treatments for SCLC.

2. MATERIALS AND METHODS

2.1. Peptide and Reagents. Octreotide (i.e., Oct) was purchased from GL Biochem (Shanghai, China, Co). N-succinimidyl-3-(trimethylstannyl)-benzoate (i.e., m-MeATE, 98%) was purchased from Toronto Research Chemicals.

N-chlorosuccinimide (NCS, 98%) was purchased from Acros (Belgium). Sephadex G-10 was purchased from GE Healthcare. The chemical reagents used were all analytical or chromatography grade.

2.2. ^{211}At Production and Radiolabeling. Astatine-211 was produced via the ^{209}Bi (α, 2n)^{211}At nuclear reaction by irradiating an internal bismuth target with α-particles accelerated to 28 MeV using a CS-30 cyclotron at Sichuan University.[37,38] The single separation yield of ^{211}At was 550−740 MBq, and the radioactivity was detected by dose calibrator (CRC-15R, American. Inc.).

The radiolabeling of Oct with ^{211}At was carried out using a previously described direct astatination procedure.[36] Briefly, Oct (5 mg/mL) was conjugated to m-MeATE (26 mmol/L in DMSO) in 0.1 mol/L phosphate-buffered saline (PBS, pH 7.6). The mixture was incubated at room temperature for 2 h. The conjugate was subsequently isolated in PBS using a Sep-pak C18 solid phase extraction column (WAT020805, American. Inc.), and then adjusted to pH 5.5 by the addition of acetic acid prior to ^{211}At labeling. HPLC was performed to confirm the identity of the product of the Oct-m-MeATE conjugate. The Oct-m-MeATE conjugate was added to Na^{211}At (∼370 MBq, in methanol) solution with 20 μL of 20 mg/mL NCS in methanol solution. The reaction mixture was incubated at RT for 5 min. Finally, the labeling reaction was terminated by the addition of 20 μL of 40 mg/mL $Na_2S_2O_5$ aqueous solution. The final product [^{211}At]SAB-Oct was isolated in PBS using a Sephadex G-10 column and verified by instant TLC (3 mm CHR, GE Whatman, Mobile phase: MeOH/$CHCl_3$ = 1:4; Final product: R_f = 0.1−0.2; free ^{211}At: R_f = 0.9−1.0) in a γ-counter (FH463B, China National Nuclear Corporation, Beijing, China).

2.3. In Vitro Stability, Cellular Uptake, and Cytotoxicity. The in vitro stability of [^{211}At]SAB-Oct was evaluated by incubating it in mouse serum at room temperature. Stability analysis was performed by iTLC at 1, 3, 6, 12, and 24 h, respectively.

The human SCLC cell line H446 and the human NSCLC cell line A549 were purchased from Cellcook Biotech (Guangzhou, China). Cells were cultured in RPMI-1640 media supplemented with 10% fetal calf serum (Sigma) and 1% PEST (penicillin 100 IU mL^{-1} and streptomycin 100 g mL^{-1}). Cells were incubated at 37 °C in incubators with humidified air equilibrated at 5% CO_2.

Cellular uptake of [^{211}At]SAB-Oct was evaluated in both the H446 and A549 cell lines in an identical fashion. Briefly, cell suspension was prepared in PBS at a concentration of 5×10^6 in low-bind Eppendorf tubes. Radioactivity (3.7 kBq) was added to each tube, and the cells were incubated at 37 °C for 1, 3, and 6 h (in triplicates) at moderate speed to prevent cell settling. At each time point, cells were centrifuged, and the supernatant was aspirated from cell pellets, which was followed by 2 additional rinses with ice-cold PBS. The supernatants were combined with the PBS wash and counted using a gamma counter. Cell pellets were then collected and counted for radioactivity. Nonspecific binding was determined by adding Oct (10 mg/mL) as a blocking agent in parallel.

In vitro cytotoxicity of [^{211}At]SAB-Oct was evaluated in comparison with PBS, unlabeled Oct (positive control), and free ^{211}At (negative control), using both H446 and A549 cell lines. Briefly, cells ($5-10 \times 10^3$/well) were seeded into 96-well plates 24 h before the experiment. Cells were incubated with cell culture media containing 1−5 μL of PBS, Oct (100 μg), free ^{211}At (0.37, 1.85 kBq), or [^{211}At]SAB-Oct (0.37, 1.85 kBq) at 37 °C for 24 h. After that, the media was removed, and the cells were washed twice with PBS. Fresh media (100 μL) containing 10 μL enhanced cell counting kit-8 solution was then added to each well, and the cells were incubated for 4 h.

2.4. DNA Damage of [^{211}At]SAB-Oct Using γH2AX Imaging. H446 and A549 cells were plated in 6-well plates (5×10^4/well). Cells were treated with PBS, Oct, free ^{211}At, and [^{211}At]SAB-Oct at four different doses (1.85, 3.7, 18.5, and 37 kBq) for 2 h and recovered in a fresh medium for 24 h. The

https://doi.org/10.1021/acs.molpharmaceut.3c00427
Mol. Pharmaceutics 2023, 20, 5543−5553

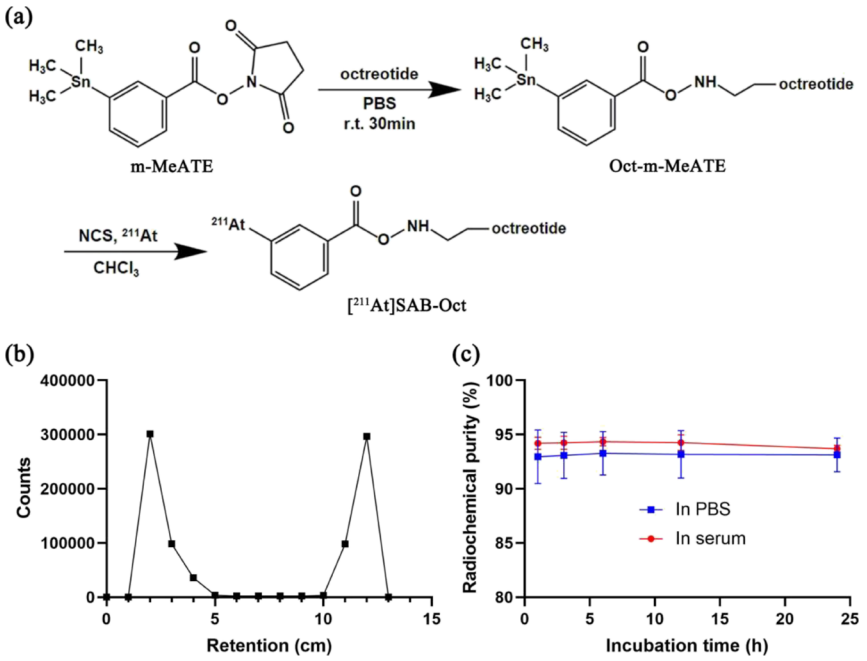

Figure 1. Synthesis and analysis of [^{211}At]SAB-Oct. (a) Synthetic scheme for [^{211}At]SAB-Oct; (b) ITLC chromatogram of [^{211}At]SAB-Oct; (c) stability over time of [^{211}At]SAB-Oct in PBS and mouse serum. Data points are the average of three independent samples, and error bars represent mean ± s.d.

cells were then washed, fixed, permeated, and stained with a mouse anti-γH2AX antibody (JBW-301 clone, 1:800).

2.5. Western Blot Analysis. Western blotting was performed as described in our previous work.[39] Cancer cells of H446 and A549 at the logarithmic growth phase, as well as H446 and A549 incubated with PBS, Oct, free ^{211}At, and [^{211}At]SAB-Oct at four different doses (1.85, 3.7, 18.5, and 37 kBq) for 2 h and recovered in fresh medium for 24 h were lysed on ice for 30 min with RIPA. The BCA Protein Assay Kit was used to calculate the quantity of protein. Equal amounts of proteins were denaturized, fractionated using 10% SDS-polyacrylamide gel electrophoresis, and then transferred to PVDF membranes. The membranes were then incubated with primary antibodies (SSTR2 antibody and γ-H2AX antibody) at 4 °C for 12 h after being blocked with 5% milk for 1 h. The protein blotting was treated with chemiluminescent (ECL) substrates after being incubated with the proper secondary antibody, and the expression levels of the proteins were then shown using an ECL detection apparatus.

2.6. Animal Experiments. All animal experiments were approved by the Animal Welfare Ethics Committee of Shanghai Tenth People's Hospital with an approval number (ID: SHDSYY-2021−3429−3711). The SCLC tumor-bearing BALB/c nude mice model was established by subcutaneously implanting H446 cells (1×10^7 cells in 0.2 mL PBS) into the left shoulder of BALB/c nude mice at 4−5 weeks of age (20 ± 1 g, both male) (Dossy Experimental Animals, Chengdu, China).

2.7. Biodistribution. The biodistributions of free ^{211}At (1110 kBq) and [^{211}At]SAB-Oct (1110 kBq) were evaluated in parallel using the BALB/c nude mice bearing subcutaneous SCLC tumors (described above, n = 4 in each group). Mice were injected with radioactivities via the tail vein and sacrificed at 1, 3, 6, 12, and 24 h. Tumor, main tissues, and whole blood were collected and weighted, and a gamma counter was used to measure ^{211}At's activity. Data were presented in percent injected dose per gram of tissue (%ID/g), except uptake in thyroid, which was presented in injected dose per organ (%ID/organ).

2.8. Therapeutic Efficacy of [^{211}At]SAB-Oct. The SCLC tumor-bearing BALB/c nude mice were established as described above and randomized into 5 groups 2 weeks after tumor inoculation. Mice were injected via the tail vein with PBS (Group A), 5 mg/kg of octreotide (B), 370 kBq of [^{211}At]SAB-Oct (C), 1110 kBq of [^{211}At]SAB-Oct (D), and 3 doses of 370 kBq of [^{211}At]SAB-Oct on Day 0, 3, and 7 (E). Mice were monitored for 30 days by measuring tumor size and body weight. Hematological indexes were detected on day 14, day 28 after the injection of Groups A,D,E, and liver and kidney function indexes were carried out on day 28 after the injection of Groups A−E. After 30 days of treatment, the random mice from each group were sacrificed, and tumors and other major organs (liver, spleen, kidney, stomach, and lung) on the mice were surgically excised, fixed with 10% (v/v) formalin, and embedded in paraffin, and stained with hematoxylin and eosin (H&E).[40]

2.9. Immunofluorescence and Immunohistochemistry. γ-H2AX was detected to evaluate DNA damage in vivo by immunofluorescence staining. Immunohistochemical staining of MHC-I and calreticulin was performed according to the manufacturer's instruction.

2.10. Statistical Analysis. Data were presented as mean ± standard deviation (s.d). Comparisons of the values between two groups used an unpaired t test. Tumor volumes were analyzed by one-way ANOVA. A P-value of <0.05 was considered significant.

3. RESULTS

3.1. Radiochemical Analyses of Radiolabeled Oct. The tin precursor for radiolabeling of ^{211}At, m-MeATE, was conjugated to Oct on the N-terminus D-phenylalanine (Figure 1a). HPLC results showed that the peaks of octreotide, m-

https://doi.org/10.1021/acs.molpharmaceut.3c00427
Mol. Pharmaceutics 2023, 20, 5543−5553

MeATE, and Oct-m-MeATE conjugate correspond to 2.28, 2.76, and 3.13 min, respectively (Figure S1).

The purified conjugate was used for radiolabeling without further purification. Radiolabeling with ^{211}At was conducted with 38−47% radiochemical yield (RCY) with greater than 90% radiochemical purity RCP (Figure 1b). The radiolabeled conjugate [^{211}At]SAB-Oct inhibited good in vitro stability in mouse serum with 93% RCP after 24 h of incubation (Figure 1c).

3.2. Cellular Uptake of [^{211}At]SAB-Oct in SSTR2-Positive Cell Lines. The H446 and A549 cell lines were reported with high levels of expression of SSTR2, which was validated upon receipt by a Western blot experiment using GAPDH as an internal standard (Figure 2a). A significantly higher expression level was seen with the H446 cell line, and hence H446 was used as a positive control while the A549, with a minimum expression of SSTR2, was used as a negative control.

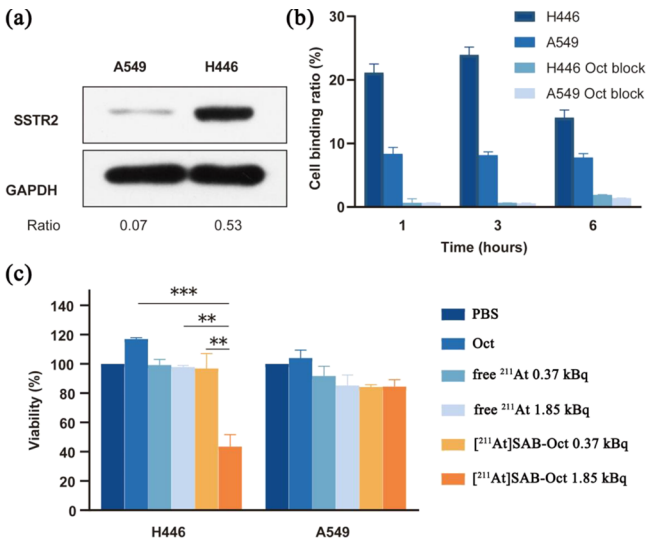

Figure 2. Cell-binding analysis in vitro by [^{211}At]SAB-Oct and subsequent cell death. (a) SSTR2 expression in H446 and A549 cells. Load control was performed using GAPDH. The images below show the ratio of SSTR2 to GAPDH intensity; (b) the binding ratio of [^{211}At]SAB-Oct to H446 and A549 cells with and without Oct block. Each experiment was conducted in triplicate (n = 3) in three independent experiments; (c) analysis of viability of cells treated for 24 h with PBS control, unlabeled Oct, free ^{211}At (0.37 or 1.85 kBq), or[^{211}At]SAB-Oct (0.37 or 1.85 kBq). There were three independent experiments conducted in triplicate (n = 3). Error bars represent mean ± s.d. (**P < 0.01 and ***P < 0.001).

Our next step was to determine if [^{211}At]SAB-Oct binds to the H446 and A549 cells. In comparison to A549 cells, the [^{211}At]SAB-Oct binding ratio to H446 cells was significantly higher. The binding ratio of [^{211}At]SAB-Oct to H446 cells was markedly decreased by 100-fold excesses of unlabeled Oct, clearly indicating the specificity of this binding (Figure 2b).

In addition, we measured the viability of H446 and A549 cells after 24 h of exposure to [^{211}At]SAB-Oct. In any case, survival was not affected by treatment with PBS, Oct, or free ^{211}At. [^{211}At]SAB-Oct doses of 1.85 kBq, however, effectively killed H446 cells and reduced their viability. According to the quantitative cell viability data, 1.85 kBq dose of [^{211}At]SAB-Oct significantly reduced H446 cell numbers compared with unlabeled octreotide (***P < 0.001), 1.85 kBq dose of free ^{211}At (**P < 0.01) (Figure 2c).

3.3. Biodistribution of [^{211}At]SAB-Oct Conjugates in Tumor-Bearing Mice. The biodistributions of free ^{211}At and [^{211}At]SAB-Oct in H446 tumor-bearing mice are summarized in Figure 3. The biodistribution analysis revealed that injected free ^{211}At was more likely to be absorbed mainly in the spleen and lung at 1 h, stomach and liver at 2 h, and then the uptake was gradually reduced within 24 h, the tumors remained at a low level of uptake for 1 to 24 h, almost similar to that of the muscle (Figure 3a).

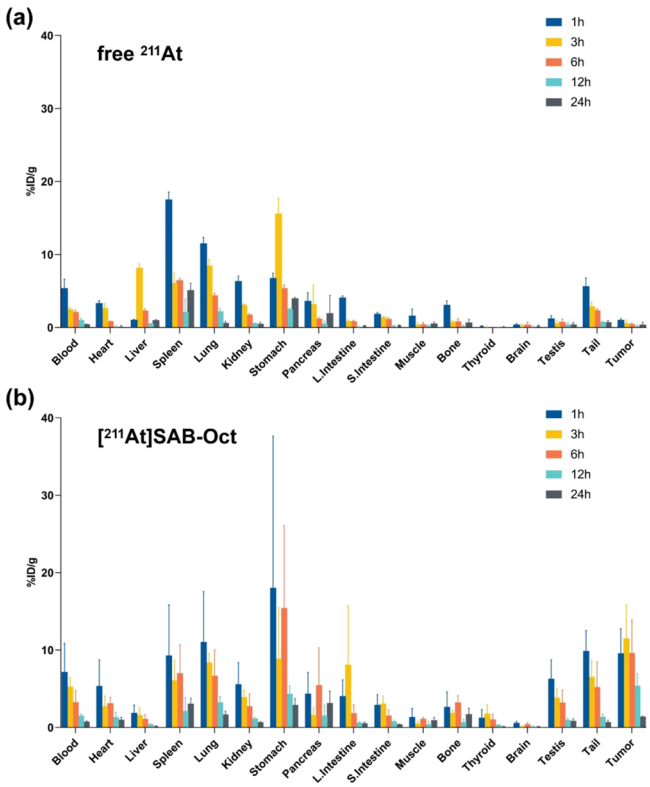

Figure 3. Biodistribution of [^{211}At]SAB-Oct in SCLC tumor-bearing BALB/c nude mice. Tumor and organ uptake of ^{211}At (%ID/g) at 1, 3, 6, 12, and 24 h after i.v. injection of (a) free ^{211}At (1110 kBq) or (b) [^{211}At]SAB-Oct (1110 kBq). Each time point involved four mice. Error bars represent mean ± s.d.

The stomach showed the highest uptake (17.99 ± 19.65% ID/g) of [^{211}At]SAB-Oct in all tissues after 1 h postinjection, and as 24 h progressed, it decreased to (2.87 ± 0.86% ID/g). The maximum tumor uptake of [^{211}At]SAB-Oct was (11.46 ± 4.35% ID/g) at 3 h postinjection. Besides, [^{211}At]SAB-Oct showed physiologically high uptake in the lung and intestines. It was observed that free ^{211}At or [^{211}At]SAB-Oct always showed low radioactivity uptake in the thyroid. Low levels of radioactivity were observed in all tissues after 24 h (Figure 3b).

3.4. DNA Damage Is Induced in Tumor Cells by [^{211}At]SAB-Oct. To uncover how [^{211}At]SAB-Oct kills tumor cells, we determined the γH2AX foci caused by DNA damage in vitro.

Treatment of cells with [^{211}At]SAB-Oct for 24 h showed clear clusters of γH2AX foci, but those treated with PBS or unlabeled octreotide showed little evidence of clusters. In H446 cells treated with [^{211}At]SAB-Oct (18.5 and 37 kBq) compared to PBS in the same group, the level of γH2AX

https://doi.org/10.1021/acs.molpharmaceut.3c00427
Mol. Pharmaceutics 2023, 20, 5543−5553

revealed a distinct dose-dependent increase(****P < 0.001). In A549 cells treated with [^{211}At]SAB-Oct (37 kBq) compared to PBS in the same group, the level of γH2AX was slightly higher (***P < 0.001), but still much lower than in H446 (***P < 0.001) (Figure 4a,b). The γH2AX expression was

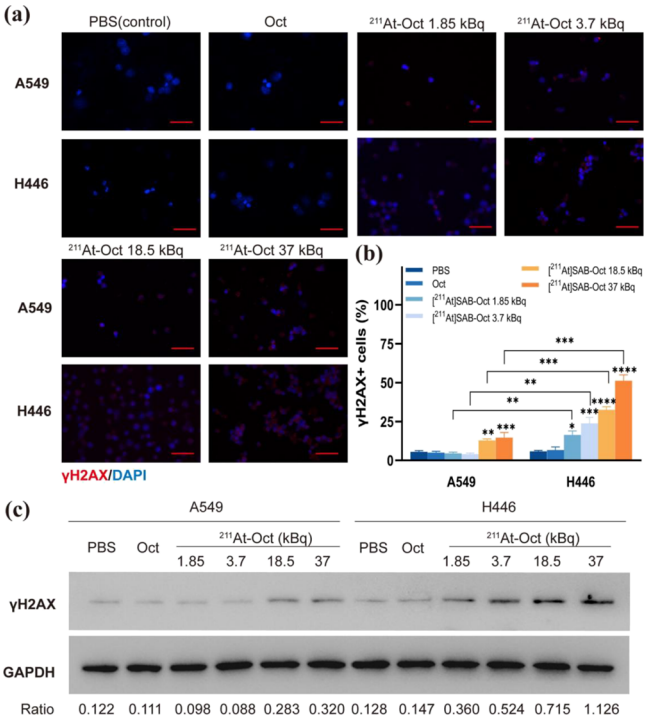

Figure 4. Images and quantitative analyses of γH2AX foci in cells following [^{211}At]SAB-Oct treatment. (a) Immunofluorescence images of γH2AX foci in A549 or H446 cells incubated with PBS, Oct or [^{211}At]SAB-Oct (1.85, 3.7, 18.5, or 37 kBq). Scale bar = 50 μm; (b) quantification of the γH2AX expression level of different groups. There were three independent experiments conducted in triplicate (n = 3). All data represent mean ± s.d. (*P < 0.01, **P < 0.01, ***P < 0.001, and ****P < 0.001); (c) Western blot analysis of γH2AX expression in A549 and NCI-446 cells incubated with PBS, Oct, or [^{211}At]SAB-Oct (1.85, 3.7, 18.5, or 37 kBq). Load control was performed using GAPDH. The images below provide ratios of γH2AX to the GAPDH band intensity.

then investigated reasonably by Western blotting test. γH2AX protein was visually increased after incubation with [^{211}At]-SAB-Oct (1.85, 3.7, 18.5, or 37 kBq) in H446 cells. In the A549 group, the protein expression of γH2AX was slightly expressed only when the dose reached 18.5 or 37 kBq (Figure 4c).

3.5. Therapeutic Efficacy of [^{211}At]SAB-Oct against SCLC Tumors in the Mice. SCLC tumor-bearing mice were divided into 5 groups. Mice received a single injection of PBS (group A), Oct (group B), [^{211}At]SAB-Oct 370 kBq (group C), [^{211}At]SAB-Oct 1110 kBq (group D), and 3 times [^{211}At]SAB-Oct with each time 370 kBq given on days 0, 3, and 7 (group E). Figure 5a shows the therapeutic effect of [^{211}At]SAB-Oct on SCLC tumors. Compared with the PBS control group, tumor growth was significantly inhibited in group C, group D with a single injection, and group E.

Blood urea nitrogen (Bun) and serum creatinine (Cr) levels are measures of renal function. On day 28, the difference in Bun and Cr concentrations were not significant (P > 0.05) between mice injected with different treatment, but for mice injected with [^{211}At]SAB-Oct 1110 kBq only a trend of decreased Bun values was observed (P > 0.05) (Figure 5c,f). Liver function is indicated by ALT and AST levels. The difference in ALT and AST concentrations were not significant (P > 0.05) between each group, AST was lower in mice of group E than in control mice on day 28 (P > 0.05) (Figure 5d,e). According to values for normal blood biochemical levels in BALB/c nude mice listed by Wuhan Saywell Biotechnology Co. Ltd., all concentrations were still within a physiological range, so impaired kidney or liver function cannot be inferred from the obtained results.

Compared with PBS control and unlabeled octreotide treated groups, we found that [^{211}At]SAB-Oct 1110 kBq acquired the highest cell necrosis, including chromatic agglutination, karyopyknosis, and nuclear fragmentation in H&E assay. Clusters of γH2AX foci were still visible in the dissected tumors of SCLC model mice on day 30 after 1110 kBq [^{211}At]SAB-Oct injection (Figure 5g).

3.6. Expression of MHC-I and Calreticulin on the Surface of Tumor Cells Was Up-Regulated by Intranuclide Irradiation. We studied the capability of ^{211}At to stimulate antitumor immunity against SCLC. Major histocompatibility complex class I (MHC-I) expression level and calreticulin expression level in SCLC tumors were examined on day 1, 4, and 8 postvarious treatments.

In the PBS group, the expression of MHC-I and calreticulin in tumor tissues was always decreased on day 1, 4, and 8 after the first administration. In the 1110 kBq administration group, the expression of MHC-I and calreticulin showed a trend of first increasing and then decreasing over time. Time-dependent increases in MHC-I and calreticulin expression were observed in the multiple-dosing group. On day 8, MHC-I and calreticulin expression reached their highest levels (***P < 0.001, **P < 0.01, respectively) (Figure 6a–d).

3.7. Adverse Effects of Injected [^{211}At]SAB-Oct in Mice Model. *3.7.1. Body Weight.* The body weight of mice was measured to determine the radioactive drug's toxicity. Although these weights tended to be lower in mice receiving 1110 kBq doses, there was no statistically significant weight change in any treatment group during the observation period (P > 0.05) (Figure 5b).

3.7.2. Assessment of Potential Impairment of Blood Cells in SCLC Tumor-Bearing Mice. To assess the potential adverse effects of [^{211}At]SAB-Oct in SCLC tumor-bearing mice, we monitored whether any changes in blood cells occurred in the treated mice. Blood cells monitoring the BALB/c nude tumor-bearing mice at day 14 and day 28 postinjection with 1110 kBq or multiple dosing [^{211}At]SAB-Oct, which revealed no significant change compared with each group (Figure 7a–f). No leukocytopenia was found in the [^{211}At]SAB-Oct 1110 kBq group on day 28. The blood plasma parameters were in the physiological range for all mice, which suggests that impaired blood cells are unlikely to be evident from the obtained results.

3.7.3. Radiation Effects on Nontargeted Tissues. According to the experimental results of the previous in vivo distribution, we carried out H&E staining analysis for nontargeted tissues that may potentially have ionizing radiation damage in groups A, D, and E.

H&E sections showed all groups' tissue liver lobule structure was clear. Occasionally, a few neutrophils gathered in the hepatic sinusoids. Slight bile duct hyperplasia was observed in a few portal areas in these three groups. No obvious morphological difference was observed. Sections of spleen

https://doi.org/10.1021/acs.molpharmaceut.3c00427
Mol. Pharmaceutics 2023, 20, 5543−5553

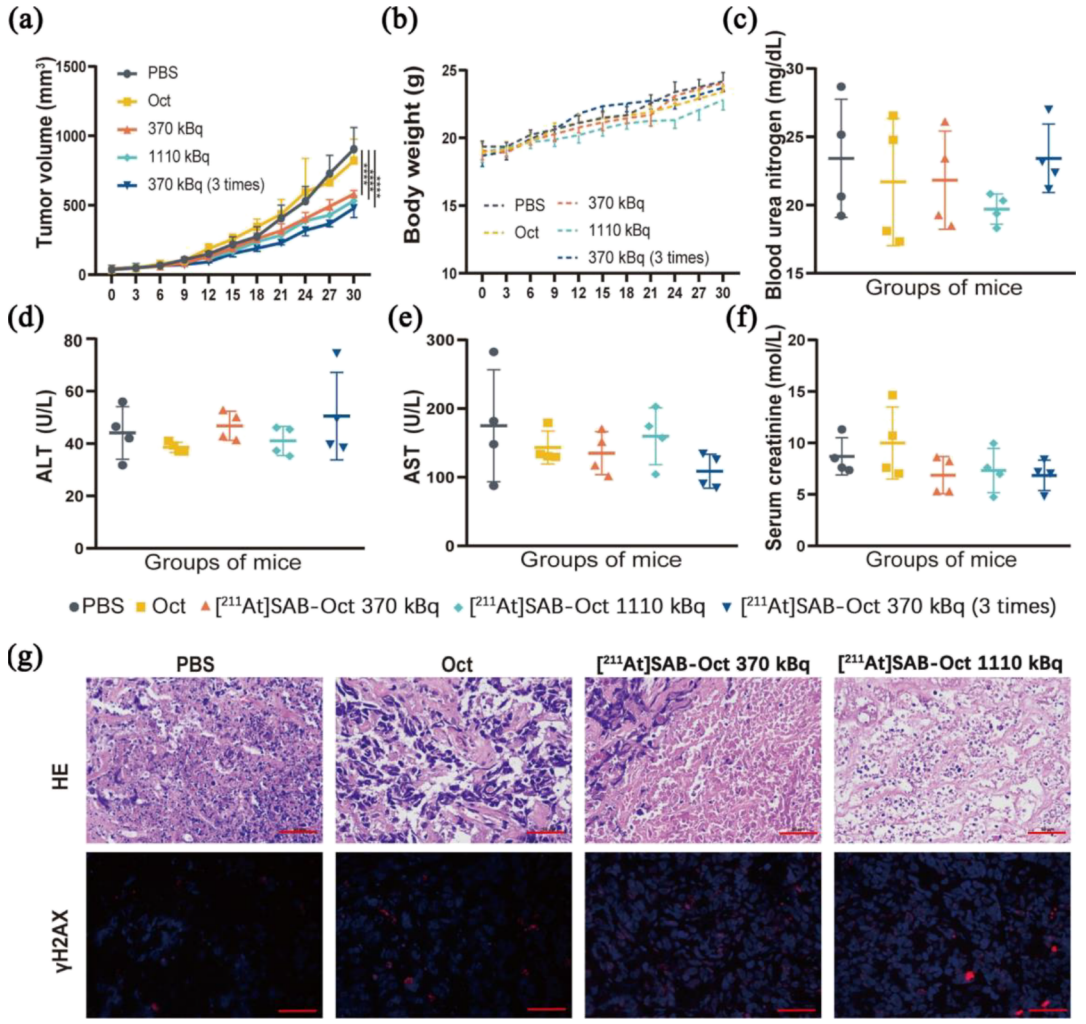

Figure 5. Therapeutic results of [^{211}At]SAB-Oct in SCLC tumor-bearing BALB/c nude mice. (a) Time-dependent tumor volume variations of SCLC tumor-bearing mice experiencing corresponding treatments in different groups. Error bars represent mean ± s.d. (n = 6−10).(****P < 0.0001); (b) body weight variations of SCLC tumor-bearing BALB/c nude mice during treatment. (n = 6−10); (c−f) liver and kidney function monitoring of the BALB/c nude mice at day 28 postinjection with PBS, unlabeled Oct, 370 kBq, 1110 kBq or multiple dosing [^{211}At]SAB-Oct. Error bars represent mean ± s.d; (g) images of H&E and γH2AX foci in SCLC tumors at day 30 postinjection with PBS, unlabeled octreotide (Oct), 370 or 1110 kBq of [^{211}At]SAB-Oct. Scale bar = 50 μm.

from groups D and E showed white pulp injury, reduced lymphocyte numbers, and more necrotic lymphocytes than those from group A. Kidney sections from groups D and E showed a few newly born renal tubular cells were observed in the local capsule of the tissue, with light cytoplasm and obvious nuclei and nucleoli. The brush border of a few renal tubular epithelial cells was slightly exfoliated. The interstitial inflammatory cells were scattered and infiltrated. In the sections of groups D and E, mild exfoliation of extensive mucosal epithelium was observed in the gastric gland area, with a disordered arrangement of local glands and more exfoliated glands. Lung H&E sections from groups A, D, and E showed no obvious abnormalities observed in the morphology and structure of tissue bronchus. Mild inflammatory cell infiltration was observed in about 50% of the alveolar walls in three groups (Figure 7g).

4. DISCUSSION

In spite of the proliferation of chemotherapy and targeted treatment options for SCLC, the prognosis of SCLC patients remains dismal. As shown in our current study, [^{211}At]SAB-Oct inhibits tumor growth as well as improves the antitumor immune response in vivo and in vitro in SSTR2-positive SCLC cells.

According to a previous study, we set various concentration doses to conduct the in vitro study.[41] Analyses of in vitro cytotoxicity revealed that [^{211}At]SAB-Oct specifically killed SSTR2-positive SCLC cells but not low-level SSTR2 A549 cells. The free ^{211}At did not affect either type of cell. In light of the fact that radiolabeled octreotide is internalized into the cells it binds to,[42,43] it appears that [^{211}At]SAB-Oct exerts its cytotoxic effects when it is bound and internalized by targeted cells. Choosing the right targeting strategy is crucial for improving the cell-killing effect of α-particle emitters.

Our in vivo biodistribution experiments showed that the tumor reached the highest aggregation of [^{211}At]SAB-Oct at the third hour after the administration, which was consistent with the half-life of the octreotide.[9,22] Although the uptake of [^{211}At]SAB-Oct in various organs decreased gradually with time delay compared with the in vivo distribution of free ^{211}At, the gastrointestinal tract showed a relatively higher uptake

https://doi.org/10.1021/acs.molpharmaceut.3c00427
Mol. Pharmaceutics 2023, 20, 5543−5553

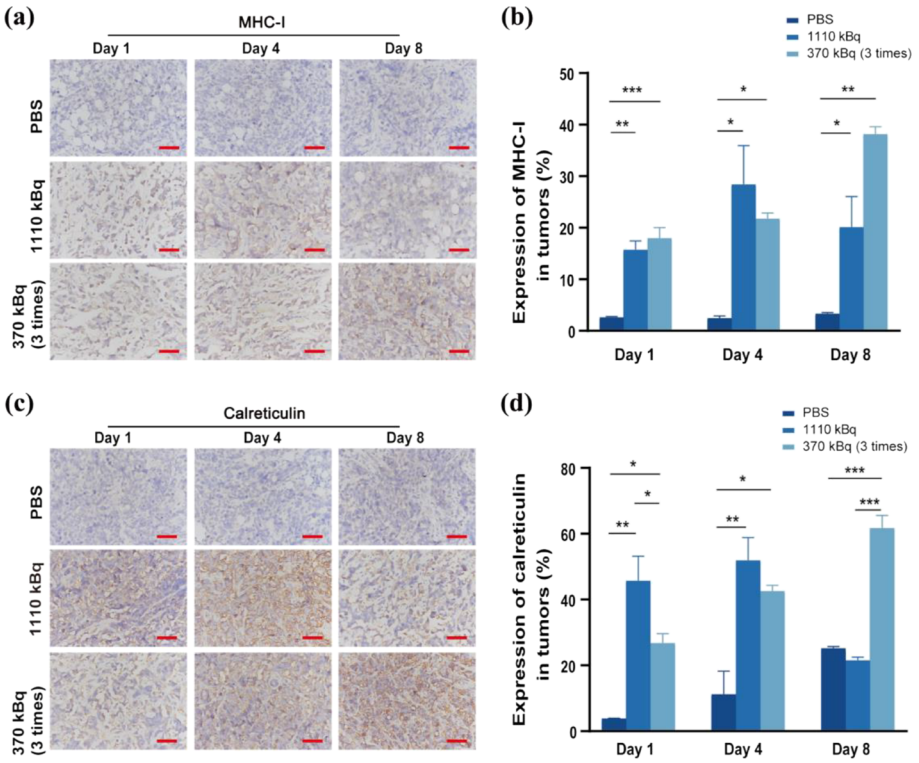

Figure 6. MHC-I and calreticulin expression level in SCLC tumor postvarious treatments at days 1, 4, 8. (a) MHC-I expression level at day 1,4,8 postinjection with PBS, 1110 kBq or multiple dosing [^{211}At]SAB-Oct. Scale bar = 50 μm; (b) quantification of the MHC-I expression level of different groups; (c) calreticulin expression level at 30 days postinjection with PBS, 1110 kBq or multiple dosing [^{211}At]SAB-Oct. Scale bar = 50 μm; (d) quantification of the calreticulin expression level of different groups. There were three independent experiments conducted in triplicate (n = 3). All data represent mean ± s.d. (**P < 0.01 and ***P < 0.001).

earlier after administration, which may be partly related to the relatively high SSTR2 expression in the digestive tract.[44−46]

Based on our current analysis, we also found that α-PRRT with [^{211}At]SAB-Oct suppressed tumor growth in SCLC tumor-bearing BALB/c nude mice. In our SCLC mice, we discovered that [^{211}At]SAB-Oct led to extensive DNA DSBs in SSTR2-positive SCLC cells, while it was not in SSTR2-low-expression A549 cells. Octreotide without labeling equal in protein content to that of the labeled octreotide could not lead to DSBs in SCLC cells. Accordingly, our hypothesis is that [^{211}At]SAB-Oct particles efficiently caused irreparable DSBs in SCLC cells and hence reduced the tumor size.

Based on our current experiments, it is clear that a single injection of [^{211}At]SAB-Oct 1110 kBq is similar to the efficiency of a multiple injection but the same amount (370 kBq × 3) to SCLC tumors. Besides, we also found that ^{211}At irradiation of SCLC tumors in vivo induced the release of MHC-I and calreticulin, considering that PRRT can not only directly cause DNA DSBs to play an antitumor role, but also change the tumor cell phenotype and microenvironment, thus inducing or regulating antitumor immune responses.[47]

The most common adverse reactions of PRRT are nephrotoxicity and myeloid toxicity.[48,49] Nephrotoxicity, usually manifested by renal dysfunction, is a major factor affecting treatment and can be combined with the use of amino acids (lysine and arginine) to protect the kidney.[50] In animal studies, enalapril maleate was used to protect the kidneys and reduce the risk of adverse reactions by speeding up drug metabolism with a diuretic.[51] In our current experiments, leukocytopenia or weight loss were not observed in mice injected with [^{211}At]SAB-Oct at 1110 kBq doses, which was consistent with a previous study.[52] Additionally, 1110 kBq [^{211}At]SAB-Oct did not significantly alter liver or kidney biochemical function in mice.

The positive expression of SSTR2 in SCLC allowed us to develop a novel SSTR2-targeting radiopharmaceutical. Earlier, ^{177}Lu-dotatate has been approved by the FDA for the treatment of gastroenteropancreatic neuroendocrine tumors (GEP-NETs). It has been shown to inhibit SSTR2-positive tumors and has emerged as a powerful alternative to octreotide in the treatment of neuroendocrine tumors.[53,54] ^{177}Lu has a short range of β-rays and little effect on normal tissues while targeting tumors.[55−57] We speculate, however, that α-rays have a shorter range and theoretically cause less radiation damage to normal tissues around tumors under the premise of precise targeting. Since β-particle-labeled somatostatin analogues have achieved better therapeutic results, α-particle ones should be more effective.

However, there are still some limitations to this research. For example, slight deastatination was observed in the spleen, lung, and stomach, which means it is necessary to introduce other substituent groups to improve the stability. In addition, the tumor volume and body weight were detected for only 30 days. They should be further observed in future studies.

5. CONCLUSIONS

We successfully constructed [^{211}At]SAB-Oct with ideal radiochemical purity and radio stability. Cell experiments showed that the viability of H446 was inhibited after the treatment of [^{211}At]SAB-Oct. The in vivo study further validated the treatment effect without causing damage to the major organs.

https://doi.org/10.1021/acs.molpharmaceut.3c00427
Mol. Pharmaceutics 2023, 20, 5543−5553

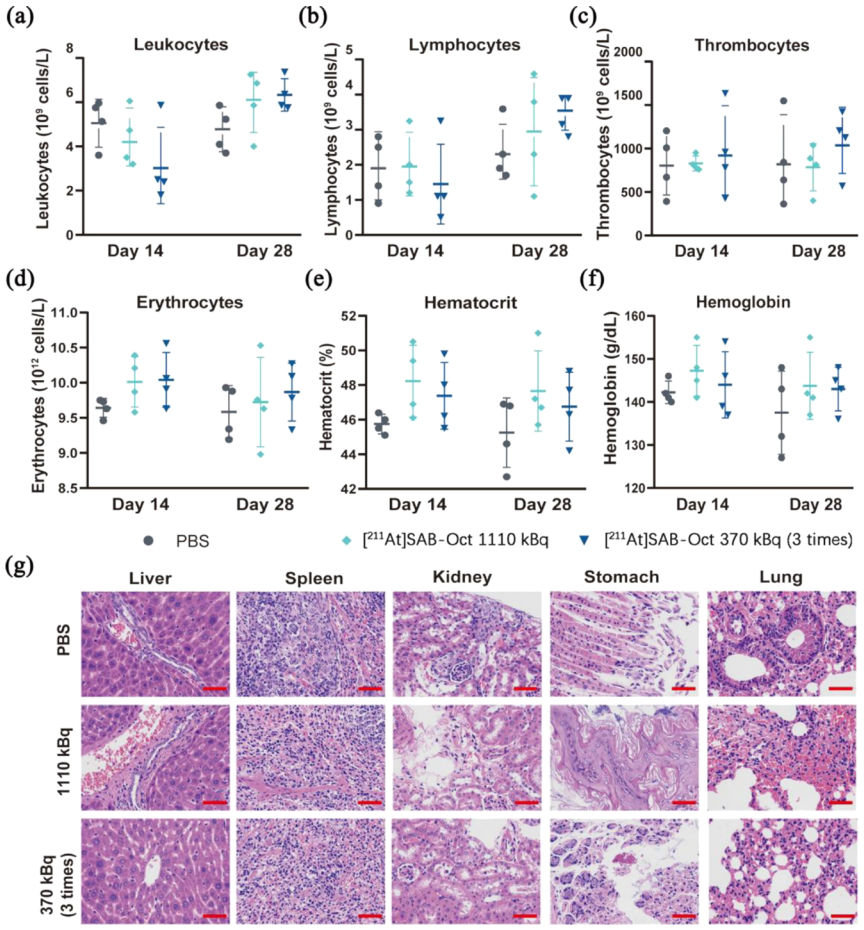

Figure 7. Side effects in SCLC tumor-bearing BALB/c nude mice treated with [^{211}At]SAB-Oct. Blood cell counts of SCLC tumor-bearing BALB/c nude mice (n = 4) on day 14 and day 28 after PBS, 1110 kBq or multiple dosing [^{211}At]SAB-Oct treatments. (a) Leukocyte counts; (b) lymphocyte counts; (c) thrombocyte counts; (d) erythrocyte counts; (e) hematocrit; (f) hemoglobin concentrations; (g) analysis of major organs in different treatment groups at day 30 postinjection with PBS, 1110 kBq or multiple dosing group. Scale bar = 50 μm.

More significantly, [^{211}At]SAB-Oct induced immunogenic cell death, indicating that it could promote antitumor responses. These properties of [^{211}At]SAB-Oct suggested its potential use as a novel adjuvant therapeutic method in conjunction with immunotherapy for the treatment of SCLC.

■ ASSOCIATED CONTENT

Data Availability Statement

Not applicable.

Supporting Information

The Supporting Information is available free of charge at https://pubs.acs.org/doi/10.1021/acs.molpharmaceut.3c00427.

HPLC chromatograms of a mixture of octreotide, m-MeATE, and Oct-m-MeATE conjugate (PDF)

■ AUTHOR INFORMATION

Corresponding Author

Fei Yu − *Department of Nuclear Medicine, Shanghai Tenth People's Hospital and Institute of Nuclear Medicine, Tongji University School of Medicine, Shanghai 200072, People's Republic of China;* orcid.org/0000-0003-2951-725X; Email: yufei_021@163.com

Authors

Shanshan Qin − *Department of Nuclear Medicine, Shanghai Tenth People's Hospital and Institute of Nuclear Medicine, Tongji University School of Medicine, Shanghai 200072, People's Republic of China*

Yuanyou Yang − *Key Laboratory of Radiation Physics and Technology, Ministry of Education, Institute of Nuclear Science and Technology, Sichuan University, Chengdu 610064, People's Republic of China*

Jiajia Zhang − *Department of Nuclear Medicine, Shanghai Tenth People's Hospital and Institute of Nuclear Medicine, Tongji University School of Medicine, Shanghai 200072, People's Republic of China*

Yuzhen Yin − *Department of Nuclear Medicine, Shanghai Tenth People's Hospital and Institute of Nuclear Medicine, Tongji University School of Medicine, Shanghai 200072, People's Republic of China*

Weihao Liu − *Key Laboratory of Radiation Physics and Technology, Ministry of Education, Institute of Nuclear Science and Technology, Sichuan University, Chengdu 610064, People's Republic of China*

Han Zhang − *Department of Nuclear Medicine, Shanghai Tenth People's Hospital and Institute of Nuclear Medicine, Tongji University School of Medicine, Shanghai 200072, People's Republic of China*

https://doi.org/10.1021/acs.molpharmaceut.3c00427
Mol. Pharmaceutics 2023, 20, 5543−5553

Xin Fan − *Department of Nuclear Medicine, Shanghai Tenth People's Hospital and Institute of Nuclear Medicine, Tongji University School of Medicine, Shanghai 200072, People's Republic of China*

Mengdie Yang − *Department of Nuclear Medicine, Shanghai Tenth People's Hospital and Institute of Nuclear Medicine, Tongji University School of Medicine, Shanghai 200072, People's Republic of China*

Complete contact information is available at: https://pubs.acs.org/10.1021/acs.molpharmaceut.3c00427

Author Contributions

S.Q. and Y.Y. contributed equally to the work. Conceptualization, S.Q., Y.Y. (Yuanyou Yang) and F.Y.; methodology, S.Q., Y.Y. (Yuanyou Yang) and J.Z.; formal analysis, S.Q., Y.Y. (Yuzhen Yin) and J.Z, investigation Y.Y. (Yuzhen Yin), W.L. H.Z., X.F. and M.Y.; writing—original draft preparation, S.Q. and Y.Y. (Yuanyou Yang); writing—review and editing, S.Q., J.Z. and F.Y.; visualization, S.Q., W.L., H.Z., X.F. and M.Y.; supervision, F.Y. All authors have read and agreed to the published version of the manuscript.

Funding

This research was funded by the National Natural Science Foundation of China (82071956), and the Shanghai Anti-Cancer Association (SACA-CY22C05).

Notes

The authors declare no competing financial interest.

Ethics approval and consent to participate for all animals were provided by the animal center of Shanghai Tenth People's Hospital, and all animal experiments were approved by Animal Welfare Ethics Committee of Shanghai Tenth People's Hospital with an approval number (SHDSYY-2021−3429−3711).

REFERENCES

(1) Apar, K.; Ganti, M.; Billy, W.; Michael, B.; Collin, B.; Anne, C.; Thomas, A.; Christopher, D. Small Cell Lung Cancer, Version 2.2022. *J. Natl. Compr. Canc. Netw.* **2021**, *19*, 1441−1464.

(2) Rudin, C. M.; Brambilla, E.; Faivre-Finn, C.; Sage, J. Small-cell lung cancer. *Nat. Rev. Dis Primers* **2021**, *7* (1), 3 DOI: 10.1038/s41572-020-00235-0.

(3) Bogart, J.; Waqar, S.; Mix, M. Radiation and Systemic Therapy for Limited-Stage Small-Cell Lung Cancer. *J. Clin. Oncol.* **2022**, *40*, 661−670.

(4) Tariq, S.; Kim, S. Y.; de Oliveira, Monteiro; Novaes, J.; Cheng, H. Update 2021: Management of Small Cell Lung Cancer. *Lung* **2021**, *199* (6), 579−587.

(5) Puliani, G.; Chiefari, A.; Mormando, M.; Bianchini, M.; Lauretta, R.; Appetecchia, M. New Insights in PRRT: Lessons From 2021. *Front. Endocrinol. (Lausanne)* **2022**, *13*, No. 861434.

(6) Rindi, G.; Mete, O.; Uccella, S.; Basturk, O.; La Rosa, S.; Brosens, L. A. A.; Ezzat, S.; de Herder, W. W.; Klimstra, D. S.; Papotti, M.; Asa, S. L. Overview of the 2022 WHO Classification of Neuroendocrine Neoplasms. *Endocr. Pathol.* **2022**, *33* (1), 115−154.

(7) Fonti, R.; Panico, M.; Pellegrino, S.; Pulcrano, A.; Vastarella, L.; Torbati, A.; Giuliano, M. Heterogeneity of SSTR2 Expression Assessed by ^{68}Ga-DOTATOC PET/CT Using Coefficient of Variation in Patients with Neuroendocrine Tumors. *J. Nucl. Med.* **2022**, *63*, 1509−1514.

(8) Vaidyanathan, G.; Affleck, D.; Schottelius, M.; Wester, H.; Friedman, H.; Zalutsky, M. R. Synthesis and Evaluation of Glycosylated Octreotate Analogues Labeled with Radioiodine and ^{211}At via a Tin Precursor. *Bioconjugate Chem.* **2006**, *17*, 195−203.

(9) Chen, L. N.; Wang, W. W.; Dong, Y. J.; Shen, D. D.; Guo, J.; Yu, X.; Qin, J.; Ji, S. Y.; Zhang, H.; Shen, Q.; He, Q.; Yang, B.; Zhang, Y.; Li, Q.; Mao, C. Structures of the endogenous peptide- and selective non-peptide agonist-bound SSTR2 signaling complexes. *Cell Res.* **2022**, *32* (8), 785−788.

(10) Fani, M.; Mansi, R.; Nicolas, G. P.; Wild, D. Radiolabeled Somatostatin Analogs-A Continuously Evolving Class of Radiopharmaceuticals. *Cancers (Basel)* **2022**, *14* (5), 1172.

(11) Wangler, C.; Beyer, L.; Bartenstein, P.; Wangler, B.; Schirrmacher, R.; Lindner, S. Favorable SSTR subtype selectivity of SiTATE: new momentum for clinical [^{18}F]SiTATE PET. *EJNMMI Radiopharm. Chem.* **2022**, *7* (1), 22 DOI: 10.1186/s41181-022-00176-x.

(12) Klose, J. M.; Wosniack, J.; Iking, J.; Staniszewska, M.; Zarrad, F.; Trajkovic-Arsic, M.; et al. Administration Routes for SSTR-/PSMA- and FAP-Directed Theranostic Radioligands in Mice. *J. Nucl. Med.* **2022**, *63*, 1357−1363.

(13) Dev, I. D.; Rangarajan, V.; Puranik, A. D.; Agrawal, A.; Shah, S.; Sahay, A.; Purandare, N. C. Sporadic Cerebellar Hemangioblastoma With Strong SSTR Expression on ^{68}Ga-DOTANOC PET/CT. *Clin. Nucl. Med.* **2023**, *48*, e28−e30.

(14) Wong, T. Y.; Zhang, K. S.; Gandhi, R. T.; Collins, Z. S.; O'Hara, R.; Wang, E. A.; Vaheesan, K.; Matsuoka, L.; Sze, D. Y.; Kennedy, A. S.; Brown, D. B. Long-term outcomes following 90Y Radioembolization of neuroendocrine liver metastases: evaluation of the radiation-emitting SIR-spheres in non-resectable liver tumor (RESiN) registry. *BMC Cancer* **2022**, *22* (1), 224 DOI: 10.1186/s12885-022-09302-z.

(15) Bober, B.; Saracyn, M.; Lubas, A.; Kolodziej, M.; Brodowska-Kania, D.; Kapusta, W.; Kaminski, G. Hepatic complications of peptide receptor radionuclide therapy with Lutetium-177 and Yttrium-90 in patients with neuroendocrine neoplasm. *Nucl. Med. Rev. Cent. East. Eur.* **2022**, *25* (1), 54−61.

(16) Liu, Y.; Watabe, T.; Kaneda-Nakashima, K.; Shirakami, Y.; Naka, S.; Ooe, K.; Toyoshima, A.; Nagata, K.; Haberkorn, U.; Kratochwil, C.; Shinohara, A.; Hatazawa, J.; Giesel, F. Fibroblast activation protein targeted therapy using [^{177}Lu]FAPI-46 compared with [^{225}Ac]FAPI-46 in a pancreatic cancer model. *Eur. J. Nucl. Med. Mol. Imaging* **2022**, *49* (3), 871−880.

(17) Kavanal, A. J.; Satapathy, S.; Sood, A.; Khosla, D.; Mittal, B. R. Subclinical Hypothyroidism After ^{225}Ac-DOTATATE Therapy in a Case of Metastatic Neuroendocrine Tumor: Unknown Adverse Effect of PRRT. *Clin. Nucl. Med.* **2022**, *47* (2), e184−e186.

(18) Simon, M.; Jorgensen, J. T.; Khare, H. A.; Christensen, C.; Nielsen, C. H.; Kjaer, A. Combination of [^{177}Lu]Lu-DOTA-TATE Targeted Radionuclide Therapy and Photothermal Therapy as a Promising Approach for Cancer Treatment: In Vivo Studies in a Human Xenograft Mouse Model. *Pharmaceutics* **2022**, *14* (6), 1284.

(19) Ahenkorah, S.; Murce, E.; Cawthorne, C.; Ketchemen, J. P.; Deroose, C. M.; Cardinaels, T.; Seimbille, Y.; Fonge, H.; Gsell, W.; Bormans, G.; Ooms, M.; Cleeren, F. 3p-C-NETA: A versatile and effective chelator for development of Al^{18}F-labeled and therapeutic radiopharmaceuticals. *Theranostics* **2022**, *12* (13), 5971−5985.

(20) Batra, V.; Samanta, M.; Makvandi, M.; Groff, D.; Martorano, P.; Elias, J.; Ranieri, P.; Tsang, M.; Hou, C.; Li, Y.; Pawel, B.; Martinez, D.; Vaidyanathan, G.; Carlin, S.; Pryma, D. A.; Maris, J. M. Preclinical Development of [^{211}At]meta- astatobenzylguanidine ([^{211}At]MABG) as an Alpha Particle Radiopharmaceutical Therapy for Neuroblastoma. *Clin. Cancer Res.* **2022**, *28* (18), 4146−4157.

(21) Zhang, J.; Kulkarni, H.; Baum, R. ^{225}Ac-DOTATOC-Targeted Somatostatin Receptor alpha-Therapy in a Patient With Metastatic Neuroendocrine Tumor of the Thymus Refractory to beta-Radiation. *Clin. Nucl. Med.* **2021**, *46* (12), 1030−1031.

(22) Vaidyanathan, G.; Boskovitz, A.; Shankar, S.; Zalutsky, M. R. Radioiodine and ^{211}At-labeled guanidinomethyl halobenzoyl octreotate conjugates: potential peptide radiotherapeutics for somatostatin receptor-positive cancers. *Peptides* **2004**, *25* (12), 2087−2097.

(23) Feng, Y.; Meshaw, R.; Zhao, X. G.; Jannetti, S.; Vaidyanathan, G.; Zalutsky, M. R. Effective Treatment of Human Breast Carcinoma Xenografts with Single-Dose (211)At-Labeled Anti-HER2 Single-Domain Antibody Fragment. *J. Nucl. Med.* **2023**, *64* (1), 124−130.

(24) Delpassand, E. S.; Tworowska, I.; Esfandiari, R.; Torgue, J.; Hurt, J.; Shafie, A.; Nunez, R. Targeted alpha-Emitter Therapy with ^{212}Pb-DOTAMTATE for the Treatment of Metastatic SSTR-Expressing Neuroendocrine Tumors: First-in-Humans Dose-Escalation Clinical Trial. *J. Nucl. Med.* **2022**, *63* (9), 1326−1333.
(25) Zalutsky, M.; Reardon, D.; Pozzi, O.; Vaidyanathan, G.; Bigner, D. Targeted α-Particle Radiotherapy with ^{211}At-labeled Monoclonal Antibodies. *Nucl. Med. Biol.* **2007**, *34*, 779−785.
(26) Ballal, S.; Yadav, M. P.; Tripathi, M.; Sahoo, R. K.; Bal, C. Survival Outcomes in Metastatic Gastroenteropancreatic Neuroendocrine Tumor Patients receiving Concomitant (225)Ac-DOTATATE Targeted Alpha Therapy and Capecitabine: A Real-world Scenario Management Based Long-term Outcome Study. *J. Nucl. Med.* **2022**, jnumed.122.264043 DOI: 10.2967/jnumed.122.264043.
(27) Bezzi, C.; Mapelli, P.; Presotto, L.; Neri, I.; Scifo, P.; Savi, A.; Bettinardi, V.; Partelli, S.; Gianolli, L.; Falconi, M.; Picchio, M. Radiomics in pancreatic neuroendocrine tumors: methodological issues and clinical significance. *Eur. J. Nucl. Med. Mol. Imaging* **2021**, *48* (12), 4002−4015.
(28) Liu, W.; Ma, H.; Li, F.; Cai, H.; Liang, R.; Chen, X.; Lan, T.; Yang, J.; Liao, J.; Yang, Y.; Liu, N. PET imaging of VEGFR and integrins in glioma tumor xenografts using ^{89}Zr labelled heterodimeric peptide. *Bioorg. Med. Chem.* **2022**, *59*, No. 116677.
(29) Jiang, C.; Tian, Q.; Xu, X.; Li, P.; He, S.; Chen, J.; Yao, B.; Zhang, J.; Yang, Z.; Song, S. Enhanced antitumor immune responses via a new agent [^{131}I]-labeled dual-target immunosuppressant. *Eur. J. Nucl. Med. Mol. Imaging* **2023**, *50*, 275−286.
(30) O'Steen, S.; Comstock, M. L.; Orozco, J. J.; Hamlin, D. K.; Wilbur, D. S.; Jones, J. C.; Kenoyer, A.; Nartea, M. E.; Lin, Y.; Miller, B. W.; Gooley, T. A.; Tuazon, S. A.; Till, B. G.; Gopal, A. K.; Sandmaier, B. M.; Press, O. W.; Green, D. J. The α-emitter astatine-211 targeted to CD38 can eradicate multiple myeloma in a disseminated disease model. *Blood* **2019**, *134* (15), 1247−1256.
(31) Morris, M. J.; Corey, E.; Guise, T. A.; Gulley, J. L.; Kevin Kelly, W.; Quinn, D. I.; Scholz, A.; Sgouros, G. Radium-223 mechanism of action: implications for use in treatment combinations. *Nat. Rev. Urol.* **2019**, *16* (12), 745−756.
(32) Karimian, A.; Ji, N. T.; Song, H.; Sgouros, G. Mathematical Modeling of Preclinical Alpha-Emitter Radiopharmaceutical Therapy. *Cancer Res.* **2020**, *80* (4), 868−876.
(33) Zhang, J.; Li, F.; Yin, Y.; Liu, N.; Zhu, M.; Zhang, H.; Liu, W.; Yang, M.; Qin, S.; Fan, X.; Yang, Y.; Zhang, K.; Yu, F. Alpha radionuclide-chelated radioimmunotherapy promoters enable local radiotherapy/chemodynamic therapy to discourage cancer progression. *Biomater. Res.* **2022**, *26* (1), 44 DOI: 10.1186/s40824-022-00290-6.
(34) Tafreshi, N. K.; Pandya, D. N.; Tichacek, C. J.; Budzevich, M. M.; Wang, Z.; Reff, J. N.; Engelman, R. W.; Boulware, D. C.; Chiappori, A. A.; Strosberg, J. R.; Ji, H.; Wadas, T. J.; El-Haddad, G.; Morse, D. L. Preclinical evaluation of [(225)Ac]Ac-DOTA-TATE for treatment of lung neuroendocrine neoplasms. *Eur. J. Nucl. Med. Mol. Imaging* **2021**, *48* (11), 3408−3421.
(35) Jurcic, J. G. Targeted Alpha-Particle Therapy for Hematologic Malignancies. *Semin. Nucl. Med.* **2020**, *50* (2), 152−161.
(36) Zhao, B.; Qin, S.; Chai, L.; Lu, G.; Yang, Y.; Cai, H.; Yuan, X.; Fan, S.; Huang, Q.; Yu, F. Evaluation of astatine-211-labeled octreotide as a potential radiotherapeutic agent for NSCLC treatment. *Bioorg. Med. Chem.* **2018**, *26* (5), 1086−1091.
(37) Liu, W.; Ma, H.; Liang, R.; Chen, X.; Li, H.; Lan, T.; Yang, J.; Liao, J.; Qin, Z.; Yang, Y.; Liu, N.; Li, F. Targeted Alpha Therapy of Glioma Using ^{211}At-Labeled Heterodimeric Peptide Targeting Both VEGFR and Integrins. *Mol. Pharmaceutics* **2022**, *19* (9), 3206−3216.
(38) Liu, Y.; Watabe, T.; Kaneda-Nakashima, K.; Shirakami, Y.; Naka, S.; Ooe, K.; Toyoshima, A.; Nagata, K.; Haberkorn, U.; Kratochwil, C.; Shinohara, A.; Hatazawa, J.; Giesel, F. Fibroblast activation protein targeted therapy using [(177)Lu]FAPI-46 compared with [(225)Ac]FAPI-46 in a pancreatic cancer model. *Eur. J. Nucl. Med. Mol. Imaging* **2022**, *49* (3), 871−880.
(39) Yu, F.; Liu, J. B.; Wu, Z. J.; Xie, W. T.; Zhong, X. J.; Hou, L. K.; Wu, W.; Lu, H. M.; Jiang, X. H.; Jiang, J. J.; Cao, Z. Y.; Cong, G. J.; Shi, M. X.; Jia, C. Y.; Lu, G. X.; Song, Y. C.; Chai, L.; Lv, Z. W.; Wu, C. Y.; Ma, Y. S.; Fu, D. Tumor suppressive microRNA-124a inhibits stemness and enhances gefitinib sensitivity of non-small cell lung cancer cells by targeting ubiquitin-specific protease 14. *Cancer Lett.* **2018**, *427*, 74−84.
(40) Zhang, J.; Yang, M.; Fan, X.; Zhu, M.; Yin, Y.; Li, H.; Chen, J.; Qin, S.; Zhang, H.; Zhang, K.; Yu, F. Biomimetic radiosensitizers unlock radiogenetics for local interstitial radiotherapy to activate systematic immune responses and resist tumor metastasis. *J. Nanobiotechnol.* **2022**, *20* (1), 103 DOI: 10.1186/s12951-022-01324-w.
(41) Li, H. K.; Morokoshi, Y.; Nagatsu, K.; Kamada, T.; Hasegawa, S. Locoregional therapy with α-emitting trastuzumab against peritoneal metastasis of human epidermal growth factor receptor 2-positive gastric cancer in mice. *Cancer Sci.* **2017**, *108* (8), 1648−1656.
(42) Li, H. K.; Morokoshi, Y.; Nagatsu, K.; Kamada, T.; Hasegawa, S. Locoregional therapy with alpha-emitting trastuzumab against peritoneal metastasis of human epidermal growth factor receptor 2-positive gastric cancer in mice. *Cancer Sci.* **2017**, *108* (8), 1648−1656.
(43) Li, H. K.; Sugyo, A.; Tsuji, A. B.; Morokoshi, Y.; Minegishi, K.; Nagatsu, K.; Kanda, H.; Harada, Y.; Nagayama, S.; Katagiri, T.; Nakamura, Y.; Higashi, T.; Hasegawa, S. α-particle therapy for synovial sarcoma in the mouse using an astatine-211-labeled antibody against frizzled homolog 10. *Cancer Sci.* **2018**, *109* (7), 2302−2309.
(44) Refardt, J.; Hofland, J.; Wild, D.; Christ, E. Molecular Imaging of Neuroendocrine Neoplasms. *J. Clin. Endocrinol. Metab.* **2022**, *107* (7), e2662−e2670.
(45) Anzola, L. K.; Rivera, J. N.; Ramirez, J. C.; Signore, A.; Mut, F. Molecular Imaging of Vulnerable Coronary Plaque with Radiolabeled Somatostatin Receptors (SSTR). *J. Clin. Med.* **2021**, *10* (23), 5515.
(46) Koustoulidou, S.; Handula, M.; de Ridder, C.; Stuurman, D.; Beekman, S.; de Jong, M.; Nonnekens, J.; Seimbille, Y. Synthesis and Evaluation of Two Long-Acting SSTR2 Antagonists for Radionuclide Therapy of Neuroendocrine Tumors. *Pharmaceuticals (Basel, Switzerland)* **2022**, *15* (9), 1155.
(47) Zhu, M.; Yang, M.; Zhang, J.; Yin, Y.; Fan, X.; Zhang, Y.; Qin, S.; Zhang, H.; Yu, F. Immunogenic Cell Death Induction by Ionizing Radiation. *Front. Immunol.* **2021**, *12*, No. 705361.
(48) Kuroda, R.; Wakabayashi, H.; Araki, R.; Inaki, A.; Nishimura, R.; Ikawa, Y.; Yoshimura, K.; Murayama, T.; Imai, Y.; Funasaka, T.; Wada, T.; Kinuya, S. Phase I/II clinical trial of high-dose [^{131}I] meta-iodobenzylguanidine therapy for high-risk neuroblastoma preceding single myeloablative chemotherapy and haematopoietic stem cell transplantation. *Eur. J. Nucl. Med. Mol. Imaging* **2022**, *49* (5), 1574−1583.
(49) Cheng, Y.; Shi, D.; Xu, Z.; Gao, Z.; Si, Z.; Zhao, Y.; Ye, R.; Fu, Z.; Fu, W.; Yang, T.; Xiu, Y.; Lin, Q.; Cheng, D. ^{124}I-Labeled Monoclonal Antibody and Fragment for the Noninvasive Evaluation of Tumor PD-L1 Expression In Vivo. *Mol. Pharmaceutics* **2022**, *19* (10), 3551−3562.
(50) Iikuni, S.; Kamei, I.; Ohara, T.; Watanabe, H.; Ono, M. Development of an ^{111}In-Labeled Glucagon-Like Peptide-1 Receptor-Targeting Exendin-4 Derivative that Exhibits Reduced Renal Uptake. *Mol. Pharmaceutics* **2022**, *19* (3), 1019−1027.
(51) Benesova, M.; Guzik, P.; Deberle, L. M.; Busslinger, S. D.; Landolt, T.; Schibli, R.; Muller, C. Design and Evaluation of Novel Albumin-Binding Folate Radioconjugates: Systematic Approach of Varying the Linker Entities. *Mol. Pharmaceutics* **2022**, *19* (3), 963−973.
(52) Mielke, C. H., Jr.; Gerich, J. E.; Lorenzi, M.; Tsalikian, E.; Rodvien, R.; Forsham, P. H. The effect of somatostatin on coagulation and platelet function in man. *N. Engl. J. Med.* **1975**, *293* (10), 480−483.
(53) Strosberg, J. R.; Caplin, M. E.; Kunz, P. L.; Ruszniewski, P. B.; Bodei, L.; Hendifar, A.; Mittra, E.; Wolin, E. M.; Yao, J. C.; Pavel, M. E.; Grande, E.; Van Cutsem, E.; Seregni, E.; Duarte, H.; Gericke, G.; Bartalotta, A.; Mariani, M. F.; Demange, A.; Mutevelic, S.; Krenning,

E. P. ^{177}Lu-Dotatate plus long-acting octreotide versus high-dose long-acting octreotide in patients with midgut neuroendocrine tumours (NETTER-1): final overall survival and long-term safety results from an open-label, randomised, controlled, phase 3 trial. *Lancet Oncol.* **2021**, *22* (12), 1752−1763.
(54) Exarchou, K.; Stephens, N. A.; Moore, A. R.; Howes, N. R.; Pritchard, D. M. New Developments in Gastric Neuroendocrine Neoplasms. *Curr. Oncol. Rep.* **2022**, *24* (1), 77−88.
(55) Muller, C.; Struthers, H.; Winiger, C.; Zhernosekov, K.; Schibli, R. DOTA conjugate with an albumin-binding entity enables the first folic acid-targeted ^{177}Lu-radionuclide tumor therapy in mice. *J. Nucl. Med.* **2013**, *54*, 124−131.
(56) Parghane, R. V.; Bhandare, M.; Chaudhari, V.; Ostwal, V.; Ramaswamy, A.; Talole, S.; Shrikhande, S. V.; Basu, S. Surgical Feasibility, Determinants, and Overall Efficacy of Neoadjuvant ^{177}Lu-DOTATATE PRRT for Locally Advanced Unresectable Gastroenteropancreatic Neuroendocrine Tumors. *J. Nucl. Med.* **2021**, *62* (11), 1558−1563.
(57) Tschan, V. J.; Borgna, F.; Busslinger, S. D.; Stirn, M.; Rodriguez, J. M. M.; Bernhardt, P.; Schibli, R.; Muller, C. Preclinical investigations using [^{177}Lu]Lu-Ibu-DAB-PSMA toward its clinical translation for radioligand therapy of prostate cancer. *Eur. J. Nucl. Med. Mol. Imaging* **2022**, *49* (11), 3639−3650.

https://doi.org/10.1021/acs.molpharmaceut.3c00427
Mol. Pharmaceutics 2023, 20, 5543−5553